Simulation of Spacecraft Sheath Impact on Langmuir Probe Measurements

Alexander Sjögren*
Embry-Riddle Aeronautical University, Daytona Beach, Fl.

Anders I. Eriksson[†] and Christopher M. Cully[‡]
Swedish Institute of Space Physics, Uppsala
(Dated: October 4, 2010)

Plasma measurements by electrostatic probes are influenced by the spacecraft-plasma interaction, including the photoelectrons emitted by the spacecraft. Such effects get particularly important in tenuous plasmas with large Debye lengths. We have used the particle-in-cell code package SPIS to study the close environment of the Rosetta spacecraft, and the impact of the spacecraft-plasma interaction on the electrostatic potential at the position of the Langmuir probes onboard. The simulations show that in the solar wind, photoemission has a bigger impact than wake formation. Spacecraft potential estimates based on Langmuir probe data in the solar wind need to be compensated for these effects when the spacecraft attitude varies. The SPIS simulations are validated by comparison to an independent code.

I. INTRODUCTION

Rosetta is an ESA mission for close inspection of the nucleus of comet 67P/Churyomov-Gerasimenko and in-situ investigations of its near environment for a period of at least one year, arriving at the comet in 2014 after a ten-year cruise through the solar system [8]. The ensemble of instruments on the spacecraft includes the two Langmuir probes of the LAP instrument [4], forming part of the Rosetta Plasma Consortium, RPC [1]. The LAP sensors are spherical probes of diameter 50 mm, mounted on short (172 mm) sticks, known as stubs, at the tips of two solid booms. In the fully developed cometary coma, plasma densities are expected to be [9] so high that the Debye length is short compared to spacecraft and boom dimensions. The high density also means that the photoemission current density for any sunlit area on the spacecraft becomes small compared to the current densities due to ram flow and random thermal motion of the plasma ions and electrons [6]. Together, these two effects of high plasma density will make direct influence of the spacecraft on LAP measurements small, at least for the boom pointing in the upstream direction of the plasma flow.

However, during the interplanetary cruise phase and at early operations at the comet, the typical plasma environment is the more or less unperturbed solar wind, in which the Debye length usually is on the order of ten meters and the photoemission saturation current dominates over the currents due to collection of plasma electrons and ions. In this situation, the contribution of plasma particles to the current to the Langmuir probes is small compared to collection of photoelectrons emitted by the spacecraft and the probe's own photoemission, so that traditional analysis of the probe characteristic for obtaining e.g. electron temperature and density is of little value. On the other hand, the low density implies that the spacecraft potential, V_s, must go positive in order to drag back sufficiently many photoelectrons and to attract plasma electrons compensating for the photoelectrons anyway lost, and V_s will then directly and sensitively depend on the plasma electron density [10]. To get a good plasma density estimate, after calibration by comparison to other data [11], we thus do not need to analyze all aspects of the Langmuir probe characteristic, just to get a value for V_s. Therefore, a scientifically useful way of operating Langmuir probes in these conditions is to use them as electric field probes, feeding them with a constant bias current to ensure that the probe remains at a stable potential with respect to its local plasma environment [12]. The measured probe-to-spacecraft potential V_ps then acts as a proxy for (the negative of) V_s, and hence for the electron density [10, 11].

With a finite boom length, the V_ps measurement will only pick up a finite fraction of V_s [2]. In addition, the measurement is complicated by contributions to the local potential in space at the probe positions from the photoelectrons, and, in supersonically flowing plasmas like the solar wind, the wake forming downstream of the spacecraft. The contributions from these sources vary with the spacecraft pointing. As long as this pointiing is stable, we can construct a locally valid calibration from V_ps to density if there are some data to compare to, as has been done for

---

*Electronic address: `sjogrena@my.erau.edu`
[†]Electronic address: `Anders.Eriksson@irfu.se`
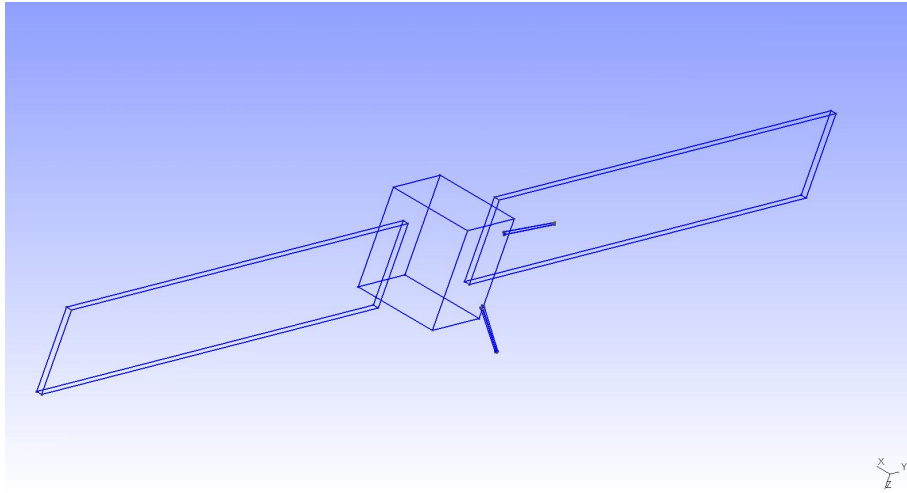[‡]Electronic address: `Chris.Cully@irfu.se`

FIG. 1: The Rosetta model used in the simulations.

Rosetta at Mars [3]. But for periods of changing pointing, we need a model of how V_{ps} depends on the spacecraft attitude, including the effects of the photoelectron cloud and the spacecraft wake, in order to reliably interpret V_{ps} in terms of plasma density. The purpose of the present study is to provide raw material for such modelling by means of particle-in-cell (PIC) simulations of Rosetta, while an attempt to synthesize a model from these simulation results is presented in an accompanying paper [5].

The PIC simulations were made with the open source SPIS package [14]. The plasma particles are represented by charged macroparticles, which interact with the electric field, and the positions of the macroparticles are calculated by solving the equations of motion. The motion is integrated with a leap-frog scheme [7], and the density is determined by linear interpolation from the positions of the macroparticles. The electric field can be derived from the charge densities and currents from the macroparticles through Poisson's equation. The linear system obtained is solved by using conjugate gradient method [15].

II. MODEL

A. Geometry

Rosetta is modelled as a cuboid (2.8x2.1x2.0 m) spacecraft body with the two booms holding the Langmuir probes attached. The solar panels stretch about 15 m in each direction (Figure 1). The LAP probes themselves and the stubs attaching them to the booms are not included in the model. Instead, we are studying the potential in the plasma at the position where the probe center would have been, thus assuming an ideal probe. The booms, 2.24 m in length for probe 1 and 1.62 m for probe 2, are held at the spacecraft potential V_s, thus bringing a fraction of the V_s to the probe position. The simulation box is chosen to be at least a couple of Debye lengths from each spacecraft surface, which after testing resulted in the box size presented in Table I. The mesh is a non-uniform mesh with smaller (about a factor 100) cell size close to the probe positions compared to the outer boundary of the box. Further details on the model can be found elsewhere [16].

All surfaces on the spacecraft are treated as being Indium Tin Oxide (ITO). For simplicity the booms are treated as emitting photoelectrons also when in shadow, as it has been shown that the effect of the photoelectrons from the booms is negligible compared to the photoelectrons from the solar panels and spacecraft body [16, Appendix E].

The solar aspect angle for the spacecraft is defined as the angle between the axis pointing towards the sun and the spacecraft x-axis (Figure 2). As the solar panels are normally kept facing the sun, the solar aspect angle is the only angle needed to describe the orientation of the spacecraft. Solar wind flow variations from the anti-sunward direction are normally small, and the preferred direction for photoemission is of course sunward, so the position of the LAP probes within the spacecraft photoelectron cloud and solar wind wake will be full specified by the solar aspect angle alone. In order to get a set of simulations for varying solar aspect angles (0-360 degrees), simulations have been done for approximately every 10 degrees.
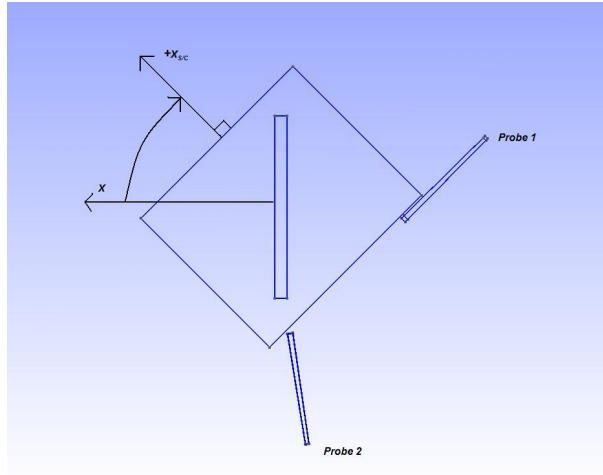
FIG. 2: The solar aspect angle is defined as the angle between the spacecraft x_{sc} axis and the direction of the sun (x), counted clockwise. In this figure the solar aspect angle is about $45\,°$.

Parameter	Value
Simulation time:	$5*10^{-4}$ s
Electron temperature, T_e:	12 eV
Ion temperature, T_i:	5 eV
Photoelectron temperature, T_{ph}:	2 eV
Plasma density, n:	5 cm^{-3}
Ion flow speed, V:	400 km/s
Spacecraft potential, V_s:	10 V
Distance to the sun, r:	1 AU
Simulation box size (x,y,z):	60x60x30 m
Characteristic length at probe position:	0.01
Characteristic length on spacecraft:	0.3
Characteristic length on simulation box:	3
Number of cells:	165,000
Number of electrons:	800,000
Number of ions:	810,000
Number of photoelectrons:	160,000

TABLE I: Simulation parameters and model details

B.   Simulation Parameters

For this study, we have run two separate sets of SPIS simulations. First, we ran a number of simulations for Rosetta in vacuum, and compared these to results from a boundary value code [2] for the same problem, as described in Section III below. For these simulations, the plasma density was set to zero, the photoemission was turned off, and the spacecraft potential (V_s) was fixed at 10 V. For the main batch of simulations, we first used nominal parameters chosen as shown in Table I. Note that the spacecraft potential is always held fixed; the potential of Rosetta in various situations have been studied by Roussel and Berthelier [13].

III.   COMPARISON WITH VACUUM MODEL

To verify the SPIS simulations, we first compared them to vacuum simulations by an independent code, using a boundary element method and previously used to study photoemission on Cluster [2]. For the corresponding SPIS simulations, the spacecraft was placed in a simulation box with no surrounding plasma and no photoelectrons. Figure

3 shows potential at probe position as a function of solar aspect angle for the two probes (blue for probe 1 and red for probe 2) for the vacuum model(thick line) and the SPIS simulations (dashed line). SPIS systematically gives a lower potential, by about 0.04 V. This difference is removed from the plots by shifting all SPIS values by +0.04 V. The compared models show good agreement, and the 180 ° periodic signature which comes from the probes being in the plane of the solar panels (held at V_s in simulations) twice per 360 ° is clearly visible also in the SPIS simulations. The boundary element method code should be the more accurate in this situation, so we can see this result as providing an error estimate on the Laplace/Poisson solver in SPIS for the grid used. For the actual plasma simulations, additional errors will result from finite number of macroparticles.

In this vacuum simulation, the variation of the potential at the probe positions is solely due to the solar panels. We find this variation to be on the order of a few percent of V_s, and as will be shown in the plasma simulations below, this is small compared to other effects.
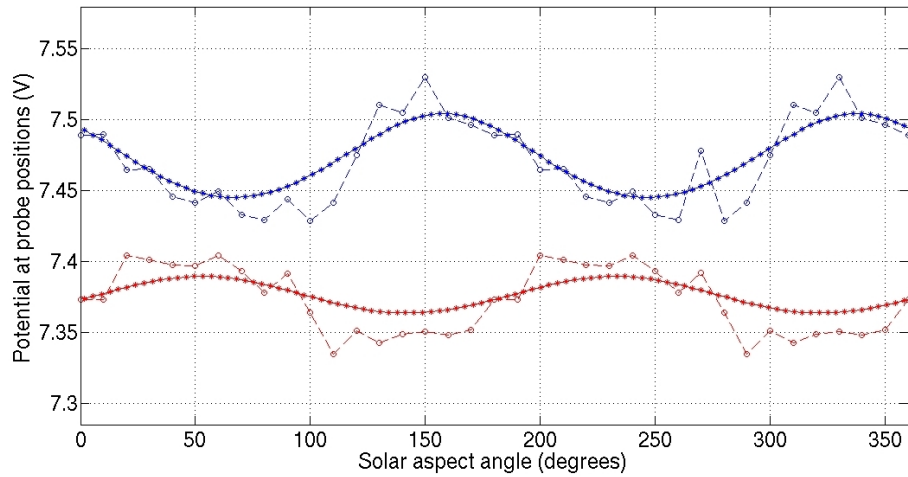

FIG. 3: Potential at probe postions (blue for probe 1, red for probe 2) for variying solar aspect angle. Comparison between code by Cully et al. [2] (thick lines) and SPIS (dashed lines - shifted +0.04 V).

IV. SIMULATION RESULTS

A. Reference simulation

Figure 4 shows the potential at the probe positions for varying solar aspect angles for simulation with parameters according to Table I, which we will use as a reference for investigating the effect of varying plasma and photoemission parameters. For probe 1 (blue) there is one major minimum of the potential at about 240 °, which is when the probe is in front of the spacecraft (compare to Figure 2), and one minor drop at 60 °, which is when the probe is behind the spacecraft. The same signatures can be seen for probe 2 at 150 ° (in front of the spacecraft) and 330 ° (behind the spacecraft), respectively. The reason for the large minimum in front of the spacecraft, which is on the order of 10 % of V_s, is the photoelectron cloud from the spacecraft body and solar panels, which can be seed in Figure 5. The smaller potential minima behind the spacecraft is caused by the ion wake formed in the flowing plasma, clearly seen in Figure 6. The effect from the wake can be seen from the plot in Figure 4 to be on the order of a few percent of V_s.

B. Variation of Solar Distance

The result of varying the solar distance is shown in Figure 7, where the potential at the probe positions is shown at 1 AU, 2 AU, and 3 AU respectively. Compared to the reference simulations in Section IV A, the intensity of the sun and the ambient plasma density are decreased by a factor $1/r^2$. Due to the decreased Debye shielding, a larger fraction of the V_s will be measured with increasing distance from the sun, and in order to compare the effects of photoelectrons and wake at various distances, the plots for $r = 2$ AU and $r = 3$ AU have been shifted -0.93 V and -1.27 V respectively in Figure 7. At $r = 2$ AU, the potential drop due to photoelectrons is on the order of 5 % of V_s, and at $r = 3$ AU it is about 3 %. The drop due to the wake is almost completely gone at solar distances larger
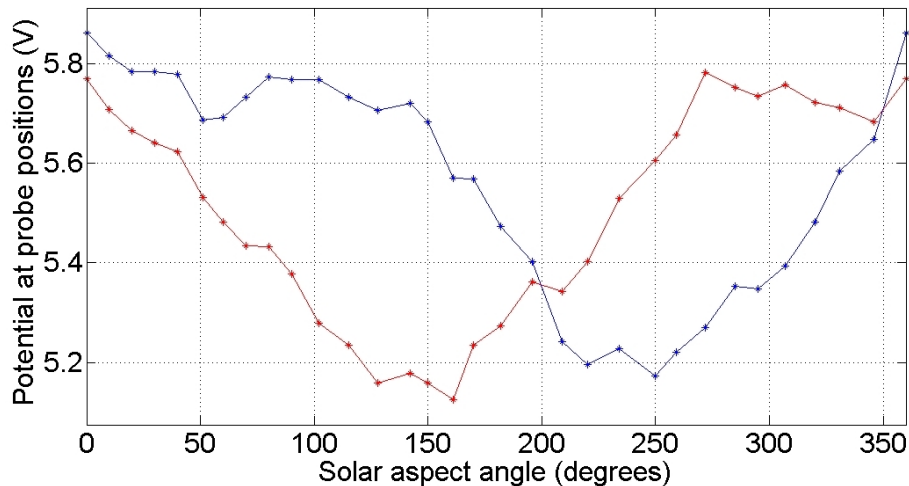
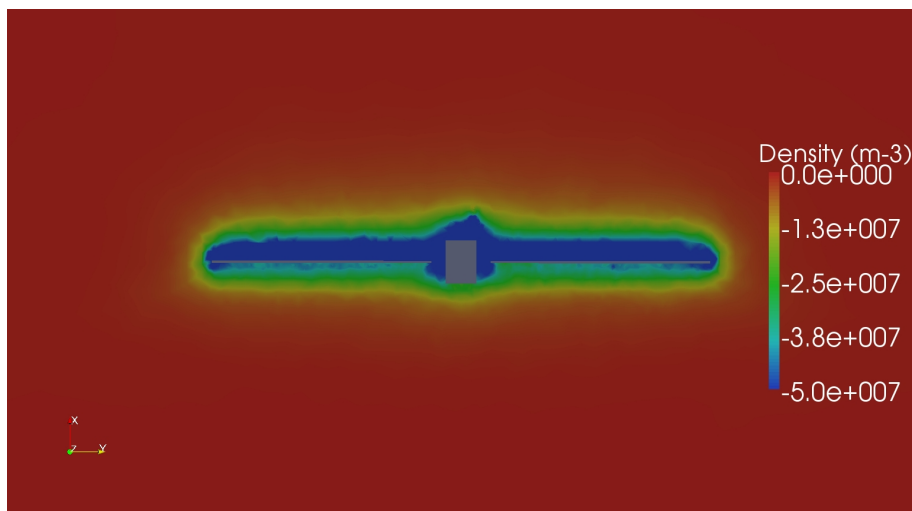FIG. 4: Potential at probe postions (blue for probe 1, red for probe 2) for the reference simulation.

FIG. 5: Photoelectron density in the XY-plane for the reference simulation, solar aspect angle of $142°$. Sun is in the positive x-direction.

than 2 AU. The results show how the the studied effects on the measured potential is decreased with increasing solar distance.

C.   Variation of Spacecraft Potential

The effect of lower spacecraft potential, V_s, was studied by keeping it locked at 5 V instead of the reference value of 10 V. The result is shown in Figure 8, where the potential at probe position is shown both for $V_s = 10$ V and $V_s = 5$ V. The latter is shifted $+4.0$ V in order to compare the amplitude of the effects of photoelectrons and wake. The potential minimum due to the photoelectrons is on the same scale for both cases, however for the case where $V_s = 5$ V, this drop amounts to about 35 % of V_s, compared to the already mentioned 10 % for the case when $V_s = 10$ V. According to Figure 8, the minimum due to the wake is decreasing with decreasing V_s. The results show that the relative importance of the photoelectrons is increased, and the relative importance of the wake is decreased with decreasing V_s.
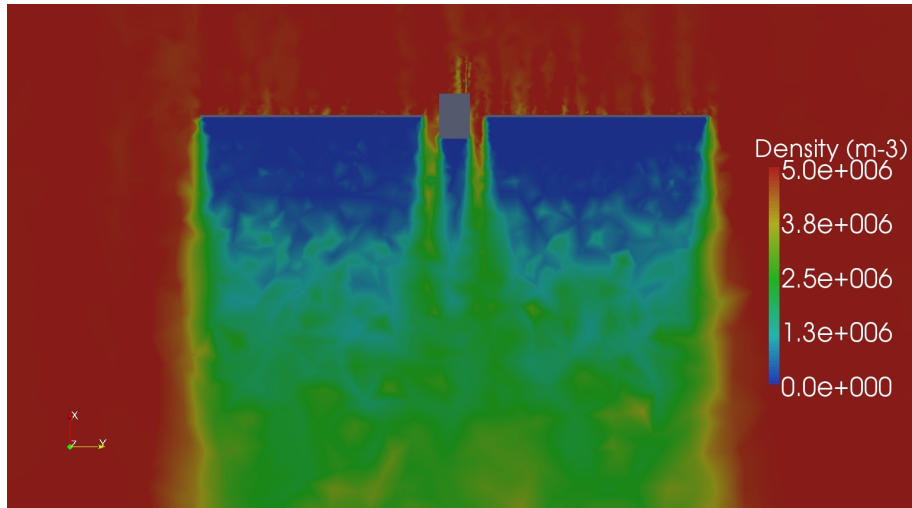
FIG. 6: Ion density in the XY-plane for the reference simulation, solar aspect angle of $142°$. Sun is in the positive x-direction.
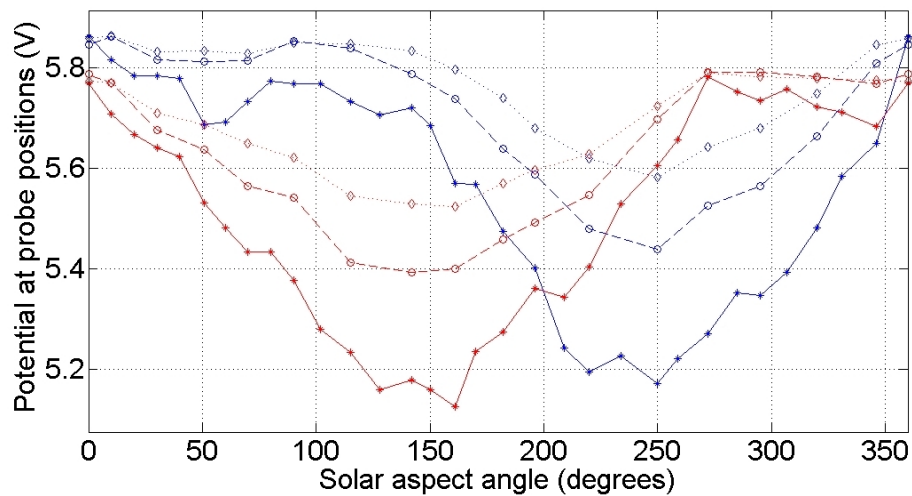

FIG. 7: Potential at probe postions (blue for probe 1, red for probe 2) for varying solar distance; $r = 1$ AU (solid), $r = 2$ AU (dashed, shifted -0.93 V), and $r = 3$ AU (dotted, shifted -1.27 V).

D. Variation of Photoelectron Temperature

To study the importance of varying photoelectron temperature (T_{ph}) for the probe measurements, simulations were made with T_{ph} at 1 eV and 4 eV, for comparison to the refernce case $T_{ph} = 2$ eV. In Figure 9 all three cases are plotted together, where the plot for $T_{ph} = 1$ eV is shifted -0.85 V and the plot for $T_{ph} = 4$ eV is shifted +0.75 V. For $T_{ph} = 4$ eV, the potential drop is on the order of 20 % of V_s, and the same value for $T_{ph} = 1$ eV is on the order of 5 %, compared to the already mentioned 10 % for $T_{ph} = 2$ eV. As expected, the potential drop due to the photoelectrons is increasing with increased photoelectron temperature.

V. CONCLUSIONS

From the simulations performed in this report, we can conclude that the wake and photoelectron cloud forming around the spacecraft indeed will influence the potential at the position of the Rosetta Langmuir probes. When plotting the simulated potential at the positions of the probes, we find that this can vary with several tenths of a volt over a complete turn of the spacecraft body around the axis of the solar panels, which we assume are always perpendicular to the sun. For typical solar wind parameters, the photoelectron cloud is seen to contribute more to
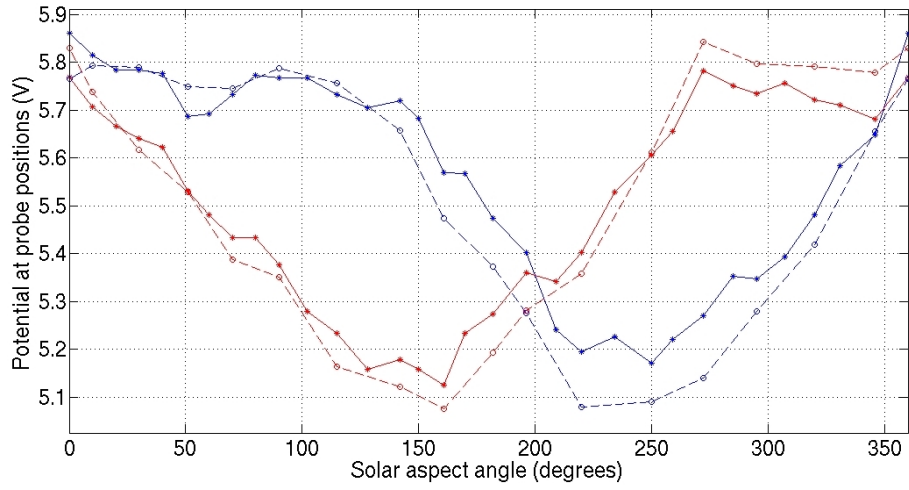
FIG. 8: Potential at probe postions (blue for probe 1, red for probe 2) for varying spacecraft potential; $V_s = 10$ V (solid) and $V_s = 5$ V (dashed, shifted +4.0 V).
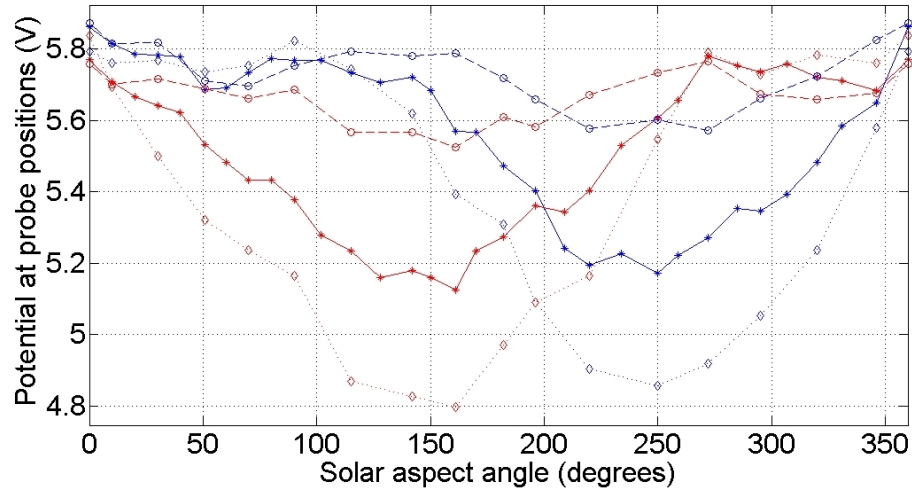

FIG. 9: Potential at probe postions (blue for probe 1, red for probe 2) for varying photoelectron temperature; $T_{ph} = 2$ eV (solid), $T_{ph} = 1$ eV (dashed, shifted -0.86 V) and $T_{ph} = 4$ eV (dotted, shifted +0.81 V).

the potential than does the spacecraft wake.

The perturbations from wake and photoelectron cloud are fully comparable in magnitude to the signal we wish to measure, i.e. the spacecraft potential variations caused by density variations in the solar wind plasma [3]. The present study can therefore be useful for establishing confidence intervals and error bars for this type of measurements. It should also be possible to construct models of the photoelectron and wake perturbations, to use for compensation for the dependence of the measured probe-to-spacecraft potential V_{ps} on spacecraft pointing. A first step towards such a model is presented in an accompanying paper [5].

Acknowledgments

AS acknowledges support from the US Air Force Research Lab for presenting this work at SCTC-11, and is also grateful to Dave Rodgers and Simon Clucas (ESA/ESTEC) for hospitality and help with getting started with SPIS.

[1] Carr, C., Cupido, E., Lee, C. G. Y., Balogh, A., Beek, T., Burch, J. L., Dunford, C. N., Eriksson, A. I., Gill, R., Glassmeier, K. H., Goldstein, R., Lagoutte, D., Lundin, R., Lundin, K., Lybekk, B., Michau, J. L., Musmann, G., Nilsson, H., Pollock, C., Richter, I., and Trotignon, J. G. (2007). RPC: The Rosetta plasma consortium. *Space Sci. Rev.*, 128:629–647, doi:10.1007/s11214–006–9136–4.

[2] Cully, C., Ergun, R. E., and Eriksson, A. I. (2007). Electrostatic structure around spacecraft in tenuous plasmas. *J. Geophys. Res.*, 112:A09211, doi:10.1029/2007JA012269.

[3] Edberg, N., Eriksson, A., Auster, U., Barabash, S., Böwetter, A., Carr, C., Cowley, S., Cupido, E., Friiz, M., Glassmeier, K.-H., Goldstein, R., Lester, M., Lundin, R., Modolo, R., Nilsson, H., Richter, I., Samara, M., and Trotignon, J. (2009). Simultaneous measurements of the martian plasma environment by Rosetta and Mars Express. *Planet. Space Sci.*, in press.

[4] Eriksson, A. I., Boström, R., Gill, R., Åhlén, L., Jansson, S.-E., Wahlund, J.-E., André, M., Mälkki, A., Holtet, J. A., Lybekk, B., Pedersen, A., Blomberg, L. G., and the LAP team (2007). RPC-LAP: The Rosetta Langmuir probe instrument. *Space Sci. Rev.*, 128:729–744, doi:10.1007/s11214–006–9003–3.

[5] Eriksson, A. I., Hånberg, C., and Sjögren, A. (2010). Modeling of spacecraft potential measurements on Rosetta. In *Proceedings of the 11th Spacecraft Charging Technology Conference (SCTC-11)*, page this volume. NASA.

[6] Eriksson, A. I. and Winkler, E. (2007). Photoemission current and solar EUV radiation: Cluster and TIMED observations. In *Proceedings of the 10th Spacecraft Charging Technology Conference (SCTC-10)*.

[7] Forest, J., Hilgers, A., Thiebault, B., Eliasson, L., Berthelier, J.-J., and de Feraudy, H. (2006). An open-source spacecraft plasma interaction simulation code PicUp3D: Tests and validations. *Plasma Science, IEEE Transactions on*, 34(5):2103–2113.

[8] Glassmeier et al., K.-H. (2007). The Rosetta mission: Flying towards the origin of the solar system. *Space Sci. Rev.*, 128:1–21, doi:10.1007/s11214–006–9140–8.

[9] Hansen, K. C., Bagdonat, T., Motschmann, U., Alexander, C., Combi, M. R., Cravens, T. E., Gombosi, T. I., Jia, Y.-D., and Robertson, I. P. (2007). The plasma environment of comet 67P/Churyumov-Gerasimenko throughout the Rosetta main mission. *Space Sci. Rev.*, 128:133–166, doi:10.1007/s11214–006–9142–6.

[10] Pedersen, A. (1995). Solar wind and magnetosphere plasma diagnostics by spacecraft electrostatic potential measurements. *Ann. Geophysicae*, 13:118–129.

[11] Pedersen, A., Lybekk, B., André, M., Eriksson, A., Lindqvist, P.-A., Mozer, F., Décréau, P. M. E., Masson, A., Laakso, H., H.Rème, Sauvaud, J.-A., Fazakerley, A., Svenes, K., Paschmann, G., Torkar, K., and Whipple, E. (2008). Electron density estimations derived from spacecraft potential measurements on Cluster in tenuous plasma regions. *J. Geophys. Res.*, 113:A07S33, doi:10.1029/2007JA012636.

[12] Pedersen, A., Mozer, F., and Gustafsson, G. (1998). Electric field measurements in a tenuous plasma with spherical double probes. In Borovsky, J., Pfaff, R., and Young, D., editors, *Measurement Techniques in Space Plasmas: Fields (AGU Geophysical Monograph 103)*, pages 1–12. American Geophysical Union.

[13] Roussel, J. and Berthelier, J. (2004). A study of the electrical charging of the Rosetta orbiter: 1. Numerical model. *Journal of Geophysical Research (Space Physics)*, 109:1104–+.

[14] Roussel, J.-F., Rogier, F., Dufour, G., Mateo-Velez, J.-C., Forest, J., Hilgers, A., Rodgers, D., Girard, L., and Payan, D. (2008). SPIS open-source code: Methods, capabilities, achievements, and prospects. *Plasma Science, IEEE Transactions on*, 36(5):2360–2368.

[15] Roussel, J.-F., Rogier, F., Volpert, D., Forest, J., Rousseau, G., and Hilgers, A. (2005). Spacecraft plasma interaction software (SPIS): Numerical solvers - methods and architecture. In *Proceedings of 9th Spacecraft Charging Technology Conference, Tsukuba, Japan*.

[16] Sjögren, A. (2009). Modelling of Rosetta langmuir probe measurements. Master's thesis, Swedish Institute of Space Physics, Uppsala, and Department of Physics and Astronomy, Uppsala University.